# The prediction of bending strengths in SFRSCC using computational fluid dynamics (CFD)

A. Orbe[a,*], R. Losada[a], E. Roji[a], J. Cuadrado[a], A. Maturana[a]

[a] *Construction Engineering Area, Department of Mechanical Engineering, Engineering Faculty of Bilbao, University of the Basque Country (UPV/EHU), Alameda Urquijo, s/n, 48013, Bilbao, Spain*

## Abstract

This research establishes a correlation between the predicted fiber orientation in Steel Fiber Reinforced Concrete (SFRC) and the flexural behavior of the composite material. It is well known that the proper alignment of fibers in the direction of tensile force enhances the mechanical properties of concrete. As recent studies have corroborated, the flow induced by self-compacting properties can influence fiber orientation. Thus, both technologies may be combined in the casting of a real-scale Steel Fiber Reinforced Self-Compacting Concrete (SFRSCC) wall (3-meters high, 6-meters long and 0.15-meter thick). Computational Fluid Dynamics (CFD) methods are applied, implementing a Bingham plastic model in a homogeneous fluid, in order to predict fiber orientation. The acceptability of the expected orientations is confirmed by analyzing the velocity fields of the fluid throughout successive time-steps of the simulation and by linking those fields to the bending strengths (pre- and post-cracking) of prismatic specimens extracted from the

*Corresponding author
*Email address:* aimar.orbe@ehu.es (A. Orbe)

wall. Expected orientations are further supported by non-destructive magnetic methods. Prediction techniques are of paramount importance nowadays, because design rules are only based on the response of preliminary prismatic specimens that are not representative of the final real structural elements. This novel methodology characterizes the material through the analysis of numerical simulations, without the cost of casting real elements, which notably simplifies the assessment of materials for use in new structural elements and geometries.

*Keywords:*

CFD, SCC, fiber orientation, strength prediction, SFRC

## 1. Introduction

Several research projects have sought to simulate material flow using various computational tools. More complex configurations are required for simulations of heterogeneous concrete matrices. In the case of Steel Fiber Reinforced Concrete (SFRC), the reinforcement is accomplished by short, discrete and randomly distributed steel fibers. The inherent difficulty of predicting and assessing fiber orientation in hardened concrete is the main drawback to its wider use. These fibers increase the tensile strength, ductility and crack-bridging capability of the composite at the expense of workability. Also, an incorrect mix-design can lead to inappropriate behavior such as fiber balling, blocking and segregation. The slender fiber shape requires more paste to avoid these sorts of disadvantages. Self-Compacting Concrete (SCC), which also improves performance, can be merged with the former technology to produce what is known as Steel Fiber Reinforced Self-Compacting Concrete

(SFRSCC). This synergy allows the application of computational techniques that simulate the composite material as a fluid. Some researchers [1] [2] have demonstrated how the tailored fresh state performance of concrete can force the fibers to align in the direction of the flow, achieving planar and, even more remarkably, unidirectional orientations.

### *1.1. Prediction*

Computational tools have the potential to reduce uncertainty. Several currents of research seek to achieve that goal, such as research into homogeneous fluid, discrete particles, and particles suspended in a medium; each with its own advantages and disadvantages [3]. Those lines of research report tests for small movements by using, for example, the slump flow test, although only very few have tested large structural elements. [4] were the first to simulate the flow of concrete, on the assumption that concrete behaves in a similar way to a homogeneous fluid. They developed the Viscoplastic Finite Element Method (VFEM) and the Divided Viscoplastic Element Methods (DVEM) for 2D flow. The free surface corresponds to the mesh deformation, in the first case, and to the displacement of virtual markers, in the second case. However, the Volume Of Fluid (VOF) method, adopted by [5] for simulating SCC casting, is the most extensively used. Slight differences when analyzing complex materials are offset by its simplicity and reduced computational cost. [6] established the Distinct Element Methods (DEM) that led to SCC flow modeling, splitting the coarse aggregate and the mortar phase [7]. Moreover, Dissipative Particle Dynamics (DPD), a mesoscopic simulation technique, has been used for simulating SCC rheology [8]. This discrete particle approach appears to model the behavior of granular

materials better than others and is more appropriate for a vibrated concrete, where the larger amount of granular particles determines the behavior of the concrete. The aggregates are coarser and are used in larger amounts than in an SCC. Nevertheless, several studies point to its suitability to simulate the flow of SCC. However, the parameters that are needed have no physical meaning. As the real behavior of SFRSCC resembles small size aggregates in a mortar paste, another alternative line of investigation is the simulation of particles suspended in a viscous medium. Those particles could also be the fibers themselves, so that their distribution and orientation could be obtained. [9] modeled aggregates as spherical particles suspended in a mortar phase, for simulating concrete flow that led to the Viscoplastic Suspended Element Method (VSEM). The studies of [10] are based on the FEMLIP method [11], integrating Lagrangian particles in an Eulerian mesh to simulate different types of concrete (normal, self-compacting, high strength) using the Bingham model. With regard to the use of fibers, [12] determined differences in fiber orientation using the slump test for Newtonian fluids and the Herschel-Bulkley model, with an Eulerian description and a modification of the Level Set Method (LSM). On the other hand, [13] adopted another way of implementing the Lattice-Boltzman model (LBM) instead of solving the Navier-Stokes equations. A modification of the Immersed Boundary Method (IBM) is used as an alternative to the VOF and the LSM methods. Despite their suitability, these methods are not sufficiently mature yet and need further development [14]. The influence of fiber orientation on the mechanical response is paramount. Based on CFD simulations, a predicted orientation can be obtained in the design stage. The consequent mechanical behavior

that is expected must be corroborated after casting, by a reliable quality control technique. This work is necessary to ensure the previously established safety coefficients. The methods summarized below, are under development for implementation in large structural elements as well as in test specimens.

### *1.2. Control*

Among the recently developed non-destructive tests (NDT), the most direct appear to be manual counting of fibers on cut faces and the application of stereological principles (Dupont and Vandewalle 2005), although these are not sufficiently practical. The correlation of electrical [15] [16] [17], magnetic [18] and signal attenuation [19] properties of the material are more suitable for indirectly assessing fiber orientation and distribution. Among those techniques is the measurement of the inductance variation of a given magnetic field, which is due to the inserted ferromagnetic fibers. Note that concrete has no influence on the magnetic field, so the measured range depends only on fiber type, amount and orientation. This paper presents a case study of the casting of a large SFRSCC wall, to examine the agreement between the expected and the real fiber orientations. Simulations of Computational Fluid Dynamics (CFD) were performed for this prediction, while magnetic methods determined the actual amount of fibers and the orientation. In parallel, aspects regarding the fiber suitability, mix-design, casting processes, testing methods (NDT or otherwise) and mechanical properties were also analyzed. According to this novel method, a remarkable link is established, by merging data, fiber orientation and residual strength, that makes it possible to predict the tensile response of the material before performing any mechanical tests. The results reported in this paper form part of a wider research project that

(a) Cast wall

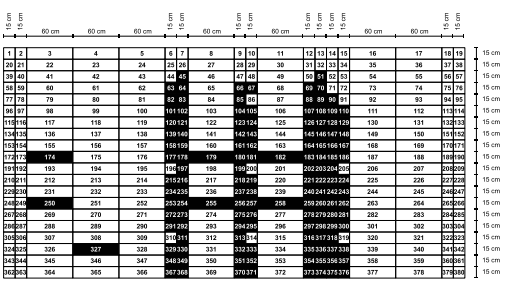

(b) Cut scheme

Figure 1: Analyzed structure and cut scheme of specimens.

is focused on the industrial applications of the material. The suitability of new structural elements and geometries can be checked in an economic way, boosting wider use of fibers in cementitious composites.

## 2. Case study

The use of real rather than laboratory-scale specimens is considered necessary, in order to work with sufficiently representative concrete movements. Hence, a real-scale 3-meter high, 6-meter long and 0.15-meter thick, SFRSCC wall was cast in situ [2]. The casting process involved pumping in the concrete from a lower corner until it had filled up the formwork. The thickness was selected based on the standardized dimension of specimens for the following tests to be performed: compression, shear, double punching, bending, permeability and magnetic tests. For that purpose, 380 prismatic (150x150x600 mm) and cubic (150x150x150 cm) specimens were cut from the wall, according to Figure 1. Their components and mix-design were adequately selected to satisfy key points relating to self-compactability, strength and durability.

## 3. Materials

Hooked-end fibers were selected from among the several fiber types found on the market, as the hook provides the necessary anchorage in the concrete matrix, transferring tensile stress, in the case of cracking. As the workability of the mass is reduced by increasing their amount, length and diameter, the fibers should be selected to achieve the best performance in both the fresh and the hardened states. Short lengths are more susceptible to slip from the matrix, but large ones make a robust and self-compacting mix-design complicated. Therefore, after suitable pull-out tests on individual fibers to verify the two preceding points, intermediate length fibers were chosen. The length and diameter of the selected fibers (HE 1/50) were 50 mm and 1 mm, respectively. The mixing procedure created a thick mixture. using an acceptable mix design based on previous experience. The proportions shown in Table 1 were determined, by taking 350 kg/m$^3$ of cement as a minimum content, in view of possible chemical attack by highly aggressive substances [20], and 0.45 as the respective maximum water/cement ratio. Even though the cement amount could be considered high, exposure to aggressive substances can be a reason to increase the minimum content. A compact granular skeleton is necessary to obtain acceptable performance (durability and strength). So, slender fibers are taken as new aggregates with a higher specific surface, which requires more mortar paste for lubrication purposes and to obtain a workable SCC. As they also interfere with the free positioning of the aggregates, it is important to search for the proportions which lead to a lower porosity. There is no one method to predict the rheological behavior of the mix and a series of characterization tests are required. In this research,

| Cement ($kg/m^3$) | Sand (0-4) ($kg/m^3$) | Gravel (4-11) ($kg/m^3$) | Plasticizer (% weight of cement) | Superplast. (% weight of cement) | Steel fibres ($kg/m^3$) | Water ($l/m^3$) |
|---|---|---|---|---|---|---|
| 434 | 1141 | 626 | 1.02 | 1.16 | 50 | 178 |

Table 1: Mix-design for the Steel Fiber Reinforced Self-Compacting Concrete (SFRSCC).

V-funnel and slump flow tests were performed to optimize the admixture amounts. A new generation of polycarboxylate ether-based superplasticizers (PCEs) was employed as high range water reducers. The final batch, prepared in the plant, showed a final spread of 710 mm ($D_f$) and needed 1.9 s to reach the 500 mm diameter line ($T_{50}$).

*3.1. Flow models*

In this study a homogeneous single-fluid approach was adopted. Concrete motion was determined by solving the Navier-Stokes equations at a constant viscosity, as shown in Equation (1), with the open-source Gerris flow solver [21]. Where an incompressible fluid is considered, mass conservation must be guaranteed, according to Equation (2).

$$\rho\left(\frac{\partial u}{\partial t} + u\nabla u\right) = -\nabla p + \nabla(2\eta|\gamma|) + \rho g \tag{1}$$

$$\nabla \cdot u = 0 \tag{2}$$

The Volume Of Fluid (VOF) technique is applied to track the free surface, which involves an adaptive mesh refinement, so that this gradient between

concrete and air is simulated. The method provides accurate adaptation to changes in topology. Depending on the values of the injected tracer, both phases can be distinguished. Each volume fraction presents properties related to the tracer values, as indicated in Equation (3a) to (3c). Tracer $c$ adopts values from 0 to 1, for air and concrete, respectively. Intermediate values show the interface or gradient of the control volume.

$$\rho = \rho_c \cdot c + .\rho_a \cdot (1 - c) \tag{3a}$$

$$\mu = \mu_c \cdot c + .\mu_a \cdot (1 - c) \tag{3b}$$

$$\tau_0 = \tau_{0,c} \cdot c + .\tau_{0,a} \cdot (1 - c) \tag{3c}$$

Fluid movements were simulated by assuming Bingham plastic behavior (Figure 2). Apparent viscosity is a basic input parameter, based on yield stress ($\tau_0$) and plastic viscosity ($\mu$). These values can be obtained with a rheometer, although [22] demonstrated that different devices show a range of different measured values. Another method involves the analysis of the slump flow test results: the final spread ($D_f$) and the time taken to pass over the 500 mm diameter circle ($T_{50}$). Yield stress is related to the maximum diameter the concrete will reach during the test, while viscosity mainly refers to the speed at which it flows. SCC shows a lower yield stress value than vibrated concrete, due to its low resistance to flow, but its viscosity is higher as it contains more fine aggregates than vibrated concrete.

Several slump flow tests were simulated in Gerris and compared with real slump tests and rheometer measurements [23]. The correlations made it possible to establish the input data ($\tau_0$ and $\mu$) needed for the proposed

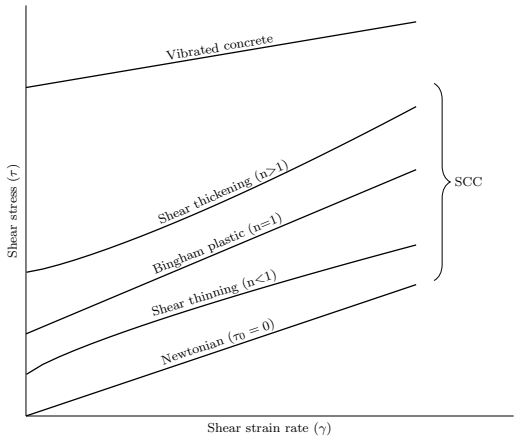


Figure 2: Rheological models.

mix-design. Unlike studies done to date, the inclusion of a slump flow test with a solid lifting cone in these simulations was notable. The mass only flows through the gap at the bottom, which increases as the cone is lifted upward, retaining any horizontal movements at the top of the slump. The parameters of the Bingham model were established from those simulations, in which the slump flow test was performed on the concrete pumped into the formwork. The final diameter ($D_f$) reached by the mass and the time it needed to arrive at a 500 mm diameter ($T_{50}$) were 710 mm and 1.9 s respectively. Those correlations suggest that the concrete should be simulated as a Newtonian fluid, rather than a Bingham plastic, with a null yield stress ($\tau_0$ = 0 Pa) and moderate viscosity ($\mu = 63$ Pas). Some authors [24] have argued that the Bingham plastic model is not the most appropriate with which to model concrete behavior. The reason for this assertion is because it gives negative yield stress values for large slumps, which is physically impossible. Hence, the preference for a Newtonian model in this study. Even though the

Bingham model underestimates shear stress, other models such as Herschel-Bulkley (shear thickening) overestimate the yield stress. In this research, the Bingham model is preferred, because its parameters have physical meaning and are easier to determine than those of the Herschel-Bulkley model.

### *3.2. Simulation set-up*

A complete model of the cast wall is represented in Figure 3, in which the main analysis centers on the 0.15 meter side boxes. These boxes are divided into 800 study units in accordance with the dimensions of the wall (length, height and thickness), although some of them are occupied by the pumping pipe. Solids are included to simulate the clamps arranged to tie both sides of the formwork, so as to consider the flow alteration that they might cause in the simulation. The concrete is pumped in at the lower left corner of the formwork through a pipe and flows from left to right and from bottom to top as the formwork fills up. The upper face is left open so that the air can escape without entrapment within the concrete.

The model implements a dynamic mesh refinement, focused on the interface and the areas of high vorticity. This adaptive refinement promotes a better approach while reducing the computational cost, providing relevant information at selected points. These application criteria are then compared with the results of the magnetic method, for which 0.15 cm side cubic specimens were used. Therefore, the study boxes have the same dimension and are only refined up for to 3 levels, when the concrete gradient passes through them or the vorticity inside is noteworthy. Figure 4 shows the basic study unit referred to as a box and its different refinement types and levels. Geometrical discontinuities, such as clamps between lateral formworks, require

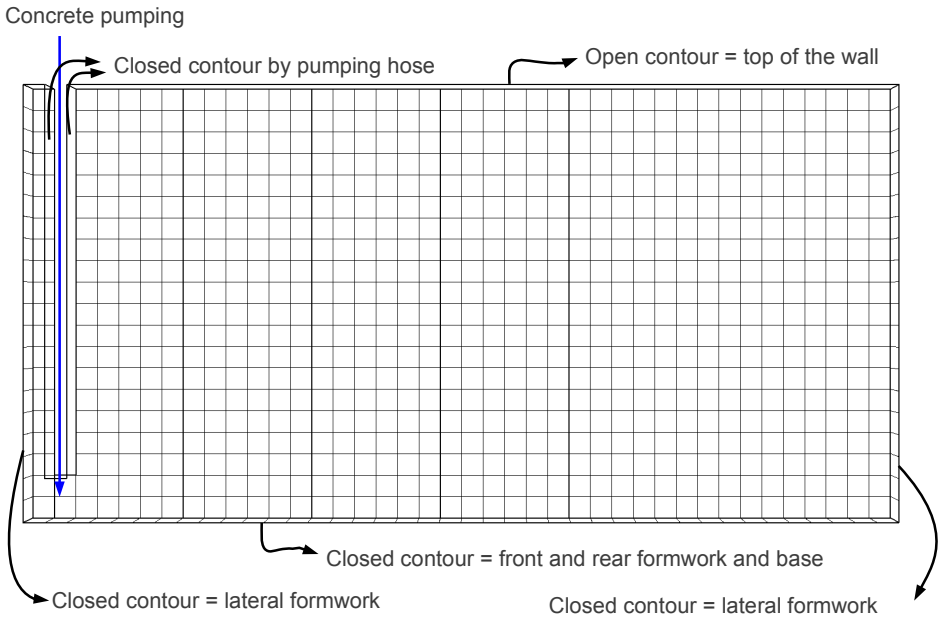


Figure 3: Simulation model and boundary conditions.

static refinement throughout the simulation, to accommodate the mesh to such small holes. On the other hand, the refinement is also dynamically performed in some areas which need a closer approach, coarsening it later where the flow is stabilized. Parallel computing with multiple processors is used, which reduces the computational cost. As a result, the position of the tracer, pressure and velocity fields of the two phases during the entire casting process were obtained for all the boxes at each time step. Since the study focuses on movement of the fresh concrete, the results of the gaseous phase are omitted. Although the procedure and the results were initially different, the simulation was adapted to the specific case under analysis. There was still a slight difference between the casting process of the wall and its simulation, as the removal of the pumping equipment was not reflected in

the latter. Pipe extraction would trigger a certain movement of the mass, especially in a vertical direction, that could change the local orientation of the fibers in the vicinity of the discharge point. However, as this was not considered very relevant for the mechanical behavior of the whole wall, it was decided to limit the simulation to the concrete pumping process. The simulation was performed in a manner that was consistent with the actual casting process, with the pumping pipe at the bottom of the formwork throughout the operation. This was not, however, the same as the previously established procedure, which determined a rate of ascent up the pipe as the concrete-air interface rose upwards. Nevertheless, casting procedures that were as real as possible were maintained in this study, as otherwise, the communication between agents is usually not as effective as expected. Consequently, the test replicated the conditions of placing concrete. The pumping rate was established, based on the time needed to complete the casting process. It took 8 minutes to fill the formwork with a volume of 2.7 m3, equivalent to a flow rate of 0.3375 m3/min. No-slip conditions were applied to the boundaries, therefore the reduced flow speed of the concrete in contact with the formwork was not considered.

## 4. Validation of expected orientations

Two velocity trends may be remarked upon during the simulation process. At the start, the unimpeded flow of concrete along the whole length and, as the volume of pumped concrete increased, boundary conditions slowed down the mass that was located furthest away from the pumping point. The restructuring of the matrix, due to the common thixotropic behavior of SCC,

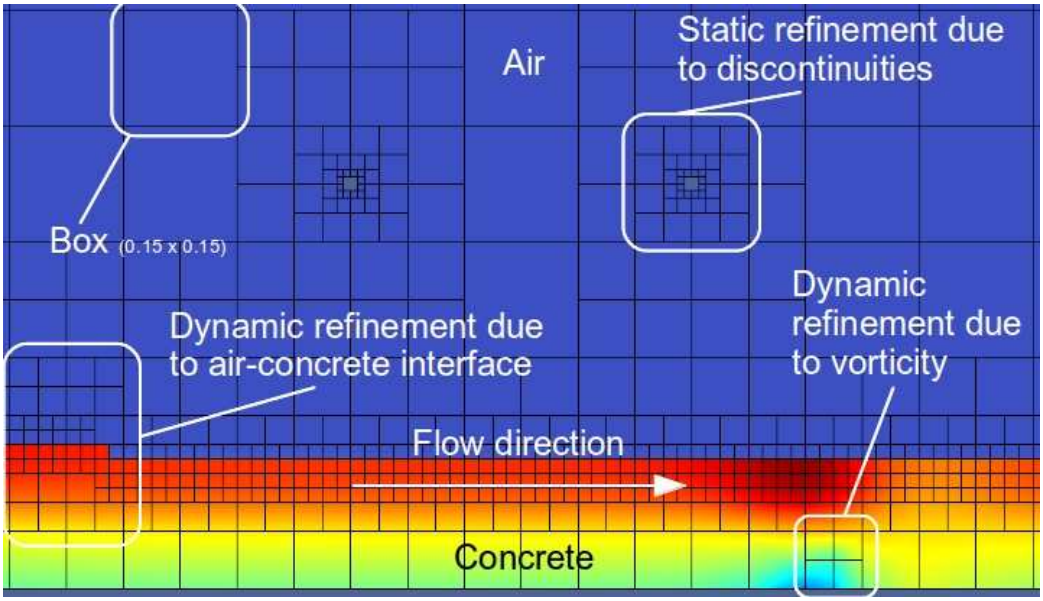


Figure 4: Refinement criteria and levels.

increased its shear strength. Therefore, the freshly pumped concrete did not have enough energy to displace the concrete that had previously been poured and to modify the trend, rising to the upper levels, as shown in Figure 5. The vertical component of the velocity vector in the proximity of the pumping pipe to the detriment of the horizontal vector is notable. The trend was reversed as the distance from the point of discharge increased and as the flow therefore stabilized. However, the higher the level where the box was located, the greater the vertical/horizontal component ratio. All the velocity fields can be analyzed for each individual box throughout the whole simulation. The tracer parameters were saved for each box at each time step. Figure 6 shows the progression of both velocity components in boxes # 85 and # 294 during the simulation. The figures focus on the time range within which the data were obtained, hence, the X-axis is discontinuous and different for each

specimen. A sketch of the position of each specimen is also provided in both cases. The horizontal velocity predominated in the lower boxes, although it tended to decrease rapidly throughout the simulation. Both components were more similar in the upper boxes and continued their displacement until the end of the pumping process. The concrete phase took longer to reach those boxes, presenting a shorter impact in the simulation than the lower ones.

These behaviors can be illustrated as an average orientation based on velocity component ratios. Thus, it is possible to compare simulation results with real orientation detected by NDT methods. Hereafter, the longitudinal direction of the wall or the X-axis is taken as the origin of the defined angles. Among the control techniques available, the most interesting one is the magnetic method. Its simplicity and the repeatability and reliability of the measurements taken have previously been demonstrated [25].

The inductance of any magnetic field is altered when a ferromagnetic material is introduced. Three different coils were built and the proportionality of the measurements, based on their self-inductance, verified. All the cubic specimens, 140 in total, were analyzed along their three axes. Besides, 7 prismatic specimens were cut into four quarters, obtaining a further 28 cubic specimens, to which magnetic methods were applied. The orientation of each axis was determined by the inductance variation value in that direction. The average of the three axes was related to the fiber amount in the specimen. The X-axis corresponds to the length of the wall, while the Z-axis corresponds to its height. The thickness or transversal direction of the wall is denoted on the Y-axis, but as expected, fewer fibers are detected along

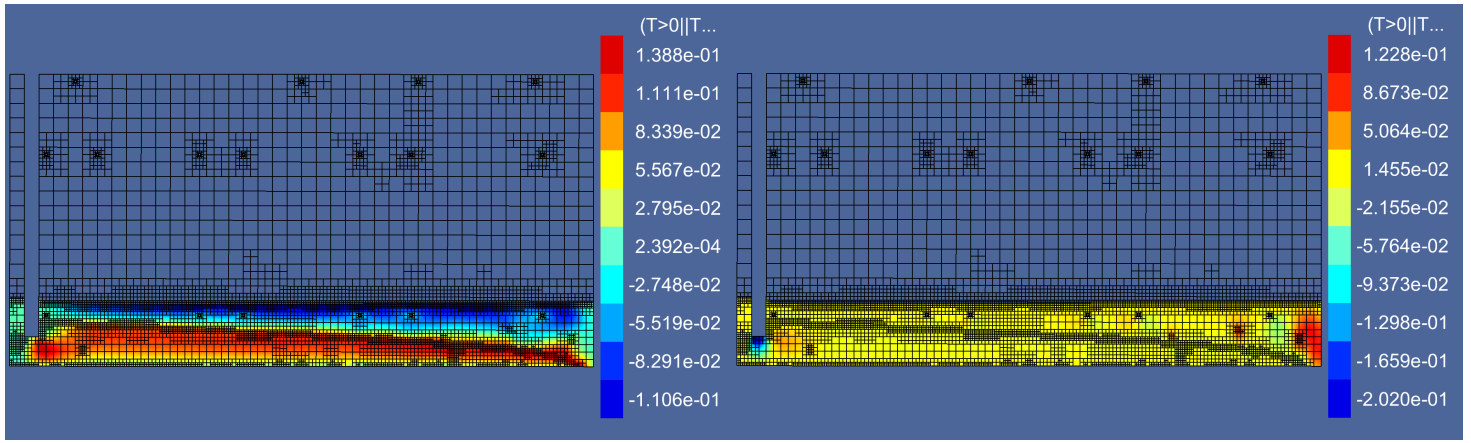


(a) Initial horizontal velocity.

(b) Initial vertical velocity.

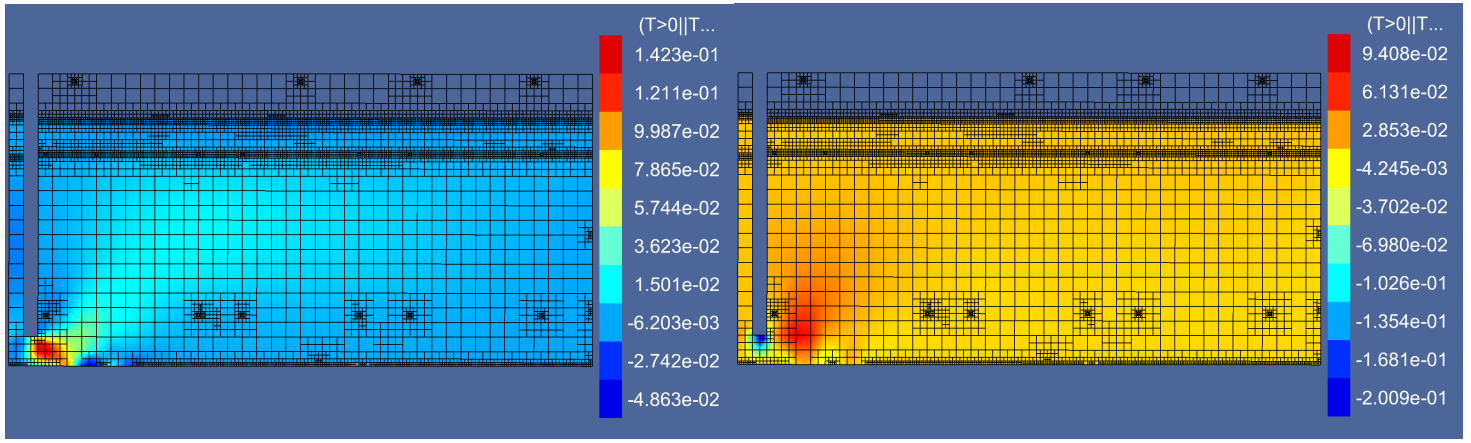


(c) Final horizontal velocity.

(d) Final vertical velocity.

Figure 5: Horizontal (left) and vertical (right) velocity fields, for initial (upper) and final (lower) time steps.

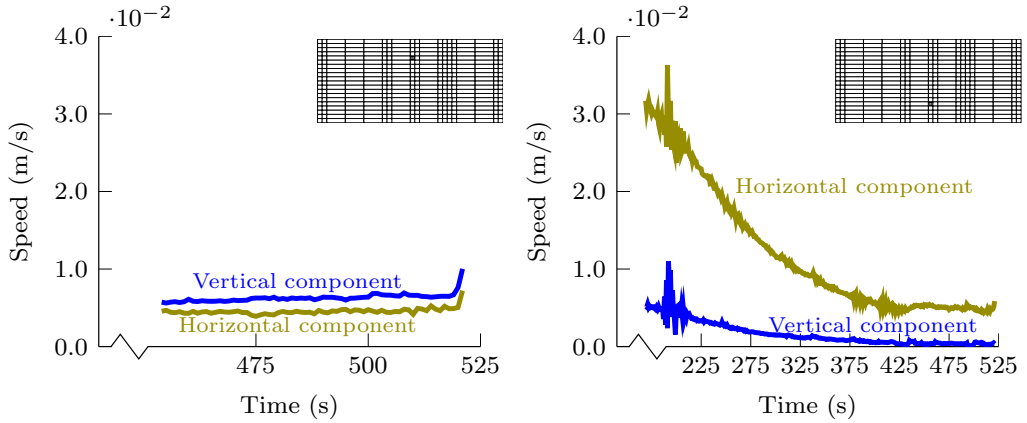


(a) Specimen # 85.

(b) Specimen # 294.

Figure 6: Progress of velocity fields for specimens # 85 and # 294.

that direction and they present fewer variations. Having such a thin wall prevents the mass from spatial flow, resulting in a two-dimensional flow as that adopted for the simulation. Figure 7 shows a superposition of both data sets for the available specimens: those from the 2D simulation and the NDT testing. With the exception of some specimens, most of them show similar behavior as expected. Note that cubic specimens are mainly analyzed, because the set-up for the magnetic method fits the cubic ones best. Prismatic specimens can only be measured on the X-axis after they have been cut into quarters. A total of 7 specimens were‘prepared and those from both sides were discarded, because a water-stop strip was attached to them and some nails arranged for fixing the wooden formwork altered the measurements. A slight segregation of fibers also occurred at the top due to some priming water in the pump, which meant that those specimens were also neglected.

The lower side presented expected orientations, mainly on the X-axis,

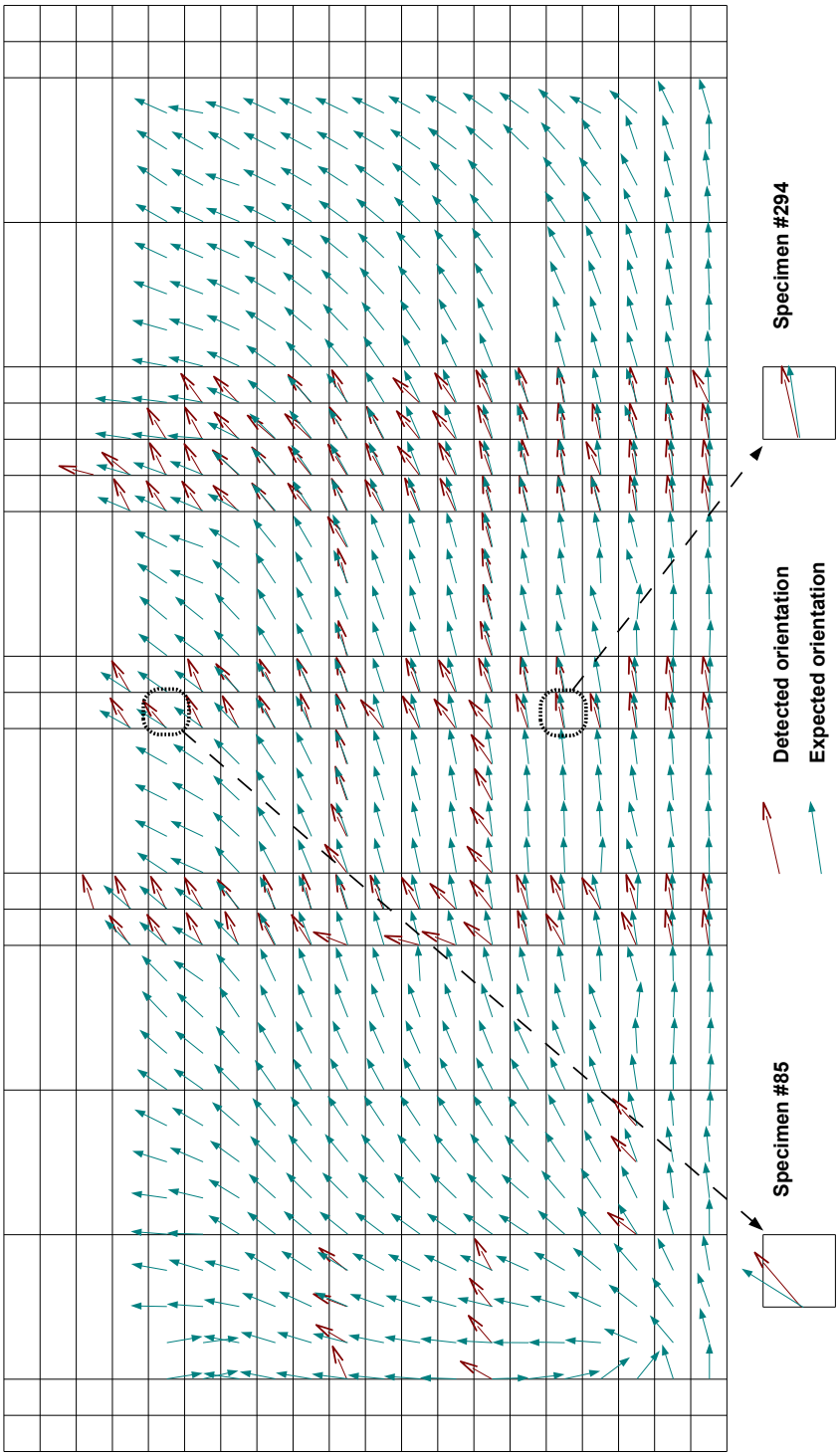


Figure 7: Superposition of predicted orientations and detected ones.

while the upper sides tended to show a more influential vertical velocity component. This agrees with previous statements. Intermediate heights exhibit variable orientations depending of the distance from the pumping pipe and their proximity to the lateral formwork, which restrains the horizontal flow of the mass (Figure 7). The distribution of fiber orientations throughout the height and the length of the wall was remarkable, as shown in Figure 8. The lower and upper parts have similar orientations throughout the wall, while intermediate rows show an uneven alignment depending on the horizontal position of the studied specimen. The reason for this uneven alignment is the transitional zone created by the vertical flow of the mass near the pumping pipe and the field of horizontal velocity in the stabilized area furthest away from the pipe. The standard deviation of the curves faithfully reflects those differences. These values vary between 12-13% for the lower and the upper rows to 32% for those in the middle.

## 5. Strength prediction

The orientation of fibers around crack planes, influences the crack-bridging potential of the material. Higher amounts of fibers aligned with the tensile direction will achieve higher strength values. Magnetic methods have already been used to verify mechanical properties of hardened SFRSCC specimens [2] as a control quality method. This study takes a step forward, predicting through the simulations the flexural response of the material. Starting from the bottom of the wall, prismatic specimens from one of every two rows have been tested according to the three-point bending test (UNE-EN 14.651). The specimens were tested as was their positions in the wall, resting on two

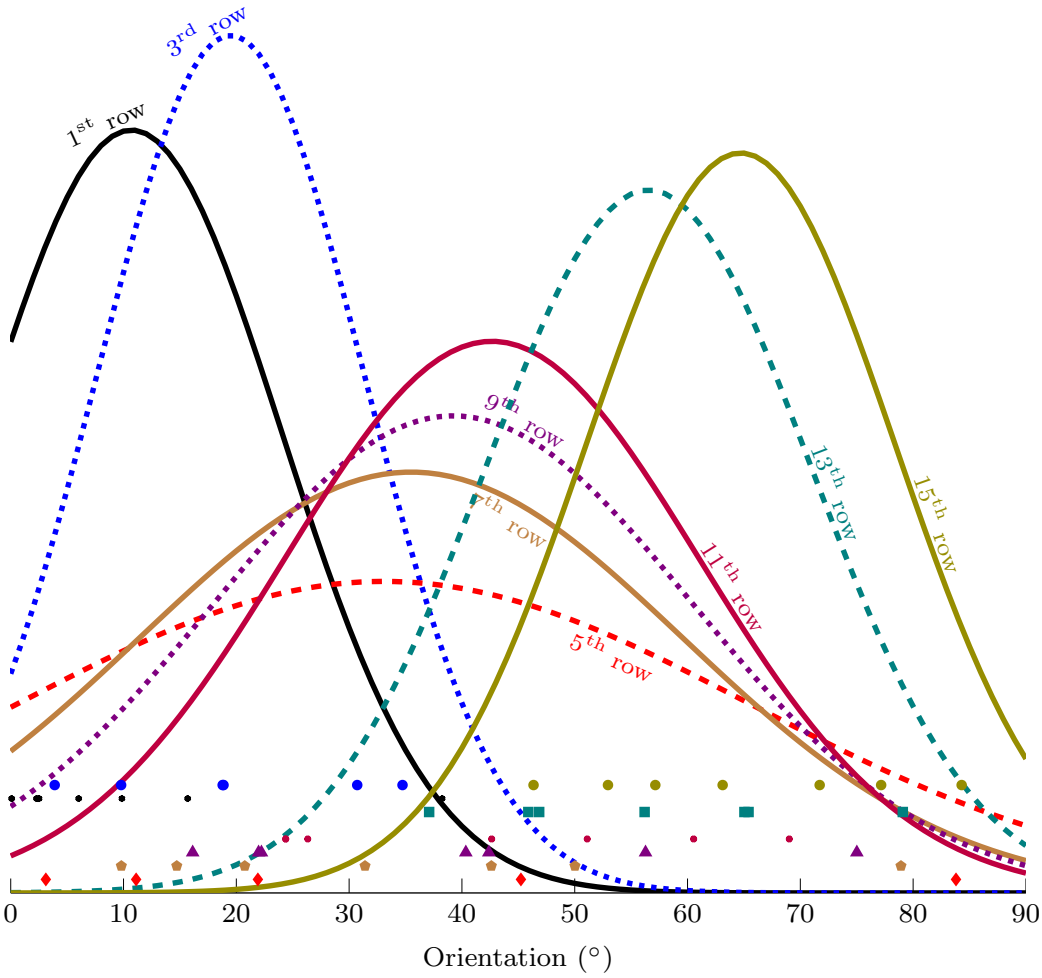


Figure 8: Gaussian distribution of orientations.

points of the lower face, while the load was applied in the center of their upper face. Tensile force developed along the longitudinal direction of the wall or its X-axis. Flexural tensile strength was measured by determining the Limit Of Proportionality (LOP) and successive residual strengths. These strengths correspond to the forces applied to obtain diverse Crack Mouth Opening Displacements (CMOD) of the notch and are the key parameters to define constitutive laws for the material, although the procedure differs between the various standards. Figure 9 illustrates the relation between fiber orientation and strength. As expected [26] [27] obtuse angles denote almost horizontal orientations providing high strength values, whereas acute angles provoke a rather brittle failure. Furthermore, it is clearly shown that the maximum values are reached for angles slightly above the horizontal plane, as [28] proven by the pull-out test on individual fibers. Matrix spalling and fiber straightening [29] increase those values. The bending test presents an inherent scatter in measured values, the variation coefficient of which can often exceed 20% [30], although it is recognized that those values decrease for larger elements. Besides, the notch required by the standard and made in the center of the lower face, cuts an unequal number of fibers in each specimen, increasing the dispersion.

$$y = A_b \cdot \frac{A_t - A_b}{\left(1 + exp^{\left(\frac{x - x_0}{w}\right)}\right)} \tag{4}$$

However, a trend line (Figures 9a to 9d) can be approximated through a sigmoid function expressed in Equation (4). The Levenberg-Marquardt algorithm (LMA) for non-linear curve fitting was applied, due to the scatter in the plotted data. This iterative procedure minimizes the square of the

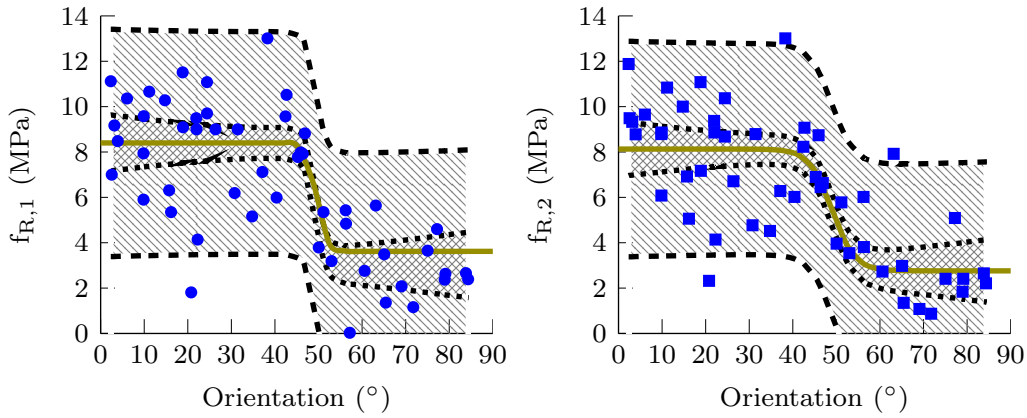


(a) $f_{R,1}$ vs. fiber orientation.

(b) $f_{R,2}$ vs. fiber orientation.

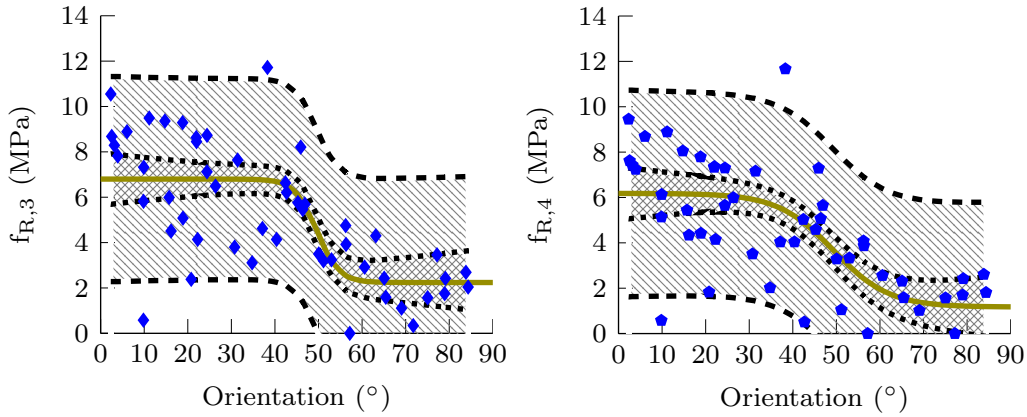


(c) $f_{R,3}$ vs. fiber orientation.

(d) $f_{R,4}$ vs. fiber orientation.

Figure 9: Prediction of residual strengths based on orientation.

deviations with the least squares method. The reliability of the defined trend line is assessed through a confidence interval, defined by two dotted lines demarcating a lined grid. The narrow confidence interval denotes a reasonably well fitted trend line. Furthermore, the dashed lines furthest from the trend line establish an area shown by oblique hatching, that requires further study. The inherent scatter in the bending test together with the results of fiber segregation offer a wide area for future study. Nonetheless, the link between residual strength and fiber orientation is quite remarkable.

The physical meaning of the parameters adopted for the equation, show useful information for understanding the behavior of the material. Its values also fit the terms of the model. $A_b$ and $A_t$ are the respective asymptotes for the function that limit the minimum and maximum values to be reached. It should be noted that this conservative approach excludes the slight increase for low inclination angles. The values $x_0$ and $w$ correspond both to the inflexion point and to the width of the transition zone from exponential growth to its deceleration and change the curvature of the function. Two distinct behaviors are separated by that imaginary border of the transition zone. Orientation with inclination angles lower than 50 degrees show an appropriate strength level, while those remarkably out of the tensile direction present lower values. The change is more abrupt for initial residual strengths, since the bearing capacity of highly inclined fibers is effective at higher crack openings. This approach is very interesting as one continuously differentiable function is sufficient to describe the strength of the material at different stages (pre- and post cracking) for any orientation. Table 2, summarizes the input data necessary to adopt the function in each case.

| Key parameter | $A_b$ (MPa) | $A_t$(MPa) | $x_0$ (°) | w (°) |
|---|---|---|---|---|
| $f_{R,1}$ | 3.02 | 8.40 | 49.42 | 1.19 |
| $f_{R,2}$ | 2.76 | 8.13 | 49.02 | 2.61 |
| $f_{R,3}$ | 2.24 | 6.80 | 49.50 | 2.55 |
| $f_{R,4}$ | 1.17 | 6.18 | 49.28 | 6.37 |

Table 2: Input parameters for predictive sigmoid function.

### *5.1. Constitutive law*

From the residual strengths obtained in the previous section, a $\sigma - \epsilon$ law can be predicted for the material. The procedure follows a four exponential approach [31] and will be compared with the diagrams plotted according the EHE-08 for the same specimens. The maximum strength reached in the pre-cracking stage is obtained as the characteristic tensile strength according to Model Code 2010. On the other hand, the tail of the curve of the diagram differs depending on the reinforcement level. The strength term governing the shape of the tail of the curve is determined according to the first residual strength of the post-cracking stage. As Figure 9a illustrates, specimens with a high angle degree present low residual strength values and those better aligned with the tensile force, higher values. Table 3 summarizes all the key parameters needed to define the behavior in both cases. Note that specimens located in the transition zone (Figure 9) are less likely to fit to the multilineal diagram.

As Figure 10 shows, the exponential approach lies usually below the established behavior defined by the destructive tests and the concrete code.

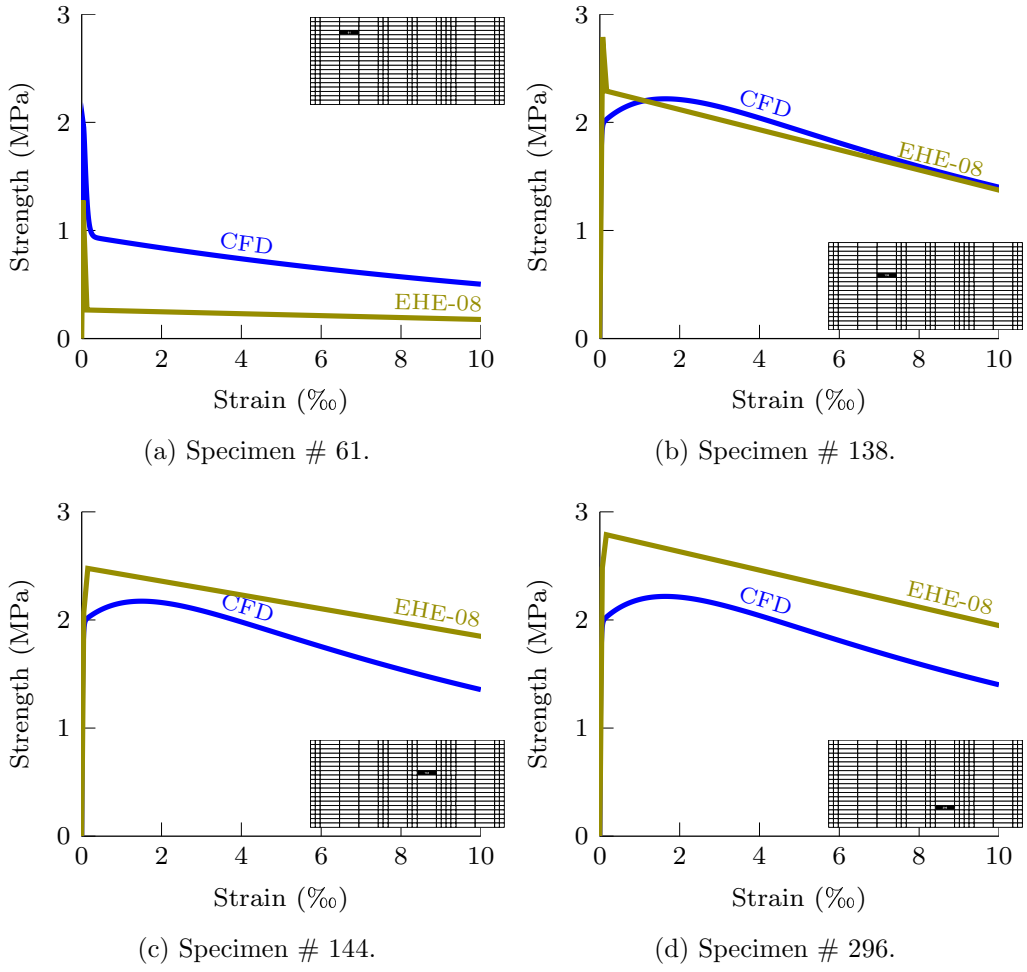


(a) Specimen # 61.

(b) Specimen # 138.

(c) Specimen # 144.

(d) Specimen # 296.

Figure 10: Multilineal diagram [20] and exponential approach.

| Stage | | $f_{pre}$ | $x_{pre}$ | $\alpha_{pre}$ |
|---|---|---|---|---|
| Pre-cracking | Fiber angle >w (°) | $f^{f}_{ct,L} = 0.21\sqrt{f^{2}_{ck}}$ | 0.01 | 100 |
| | Fiber angle <w (°) | | 0.005 | 1.001 |
| | | $f_{post}$ | $x_{post}$ | $\alpha_{post}$ |
| Post-cracking | | $f_{R,1}$ (Fig. 9a) | 0.5 | 10 |

Table 3: Kay parameters for the predicting four exponential model.

Therefore, the prediction can be considered conservative. As an exception, specimen # 61 shows a rather low strength level than what was expected. It is not due to an inaccurate estimation of the lower asymptotic limit, but to a static and dynamic segregation that occurred on the upper side of the wall. Specimens located in that area present a similar behavior. The Fiber Dynamic Segregation Index (FDSI) [32] obtained in this case, has been already analyzed [33]. The single fluid model considers an uniform fiber distribution and, therefore, reinforcement of the matrix. Even though segregation is not detected and it does not fit the exact values, the high angle that fibers present with respect to the horizontal axis, denotes the abrupt drop after matrix cracking and the consequent low residual strengths. The slight discrepancies also have their origin in the inherent scatter of the aforementioned bending test and the criteria adopted by the diverse standards, in this cases the UNE-EN 14.651, to determine the LOP and the residual strengths.

Therefore, this method allows to predict the mechanical properties of the SFRSCC, regarding its tensile behavior, and detects weak points in the structure. All this information can be obtained without having cast the

concrete and subjected it to destructive testing, providing significant time and cost savings.

## 6. Conclusions

A methodology for predicting the mechanical properties of fiber reinforced concretes under bending tests has been presented in this study. The acceptability of Computational Fluid Dynamics (CFD) has been demonstrated for simulating the flow of SFRSCC. The single homogeneous fluid approach along with the Volume of Fluid (VOF) method resulted in accurate fiber orientation prediction, at reduced computational costs. Therefore, this technique is considered capable of detecting incorrect casting procedures and weak points within the structure, prior to its actual construction. Likewise, unsuitable concrete rheologies can be ascertained from the formwork geometries that have been designed. The research has focused on a real-scale structural element, rather than a laboratory scale specimen. The motion of the mass was therefore uncertain, invalidating possible conjectures. Adoption of the proposed trend lines as calibration patterns has provided interesting design tools with which to determine the key parameters (i.e. residual strengths) established in various standards. From those key parameters and following the procedure of each standard, the constitutive law of the material can be predicted at every point of the structural element. This is essential, as fiber orientation and concrete strength, may vary considerably within the element depending on the mass flow of the concrete. This predictive procedure, allows us to determine structural areas with a inadequate reinforcement level due to incorrect alignment of fibers. Detecting weak points beforehand, increases

the security of the structures while reducing their quality control costs. Also multiple simulations can be performed, without real castings, to establish the best process to apply on site.

## Acknowledgments

The research presented in this paper was granted by the Spanish Ministry of Science and Innovation through MIVES IV ref: BIA 2010-20789-C04-04 and the Basque Regional Government through IT781-13. The authors also wish to thank ArcelorMittal-Wire Solutions and Financiera y Minera (Italcementi Group) for providing materials for the real experimental program.

## References

[1] Stähli, P., Custer, R., van Mier, J.. On flow properties, fibre distribution, fibre orientation and flexural behaviour of FRC. Materials and Structures 2008;41:189–196.

[2] Orbe, A., Cuadrado, J., Losada, R., Rojí, E.. Framework for the design and analysis of steel fiber reinforced self-compacting concrete structures. Construction and Building Materials 2012;35(0):676 – 686.

[3] Gram, A., Silfwerbrand, J.. Numerical simulation of fresh SCC flow: applications. Materials and Structures 2011;44:805–813.

[4] Tanigawa, Y., Mori, H.. Rheological analysis of slumping behavior of fresh concrete. In: Proceedings of the 29th Japan congress on materials research. 1986, p. 129.

[5] Thrane, L.N.. Form filling with self-compacting concrete. Ph.D. thesis; Technical University of Denmark; 2007.

[6] Chu, H., Machida, A.. Experimental evaluation and theoretical simulation of self compacting concrete by the Modified Distinct Element Method (MDEM). In: Recent advances in concrete technology, fourth CANMET/ACI/JCI international conference; vol. 179. 1998, p. 691–714.

[7] Mechtcherine, V., Gram, A., Krenzer, K., Schwabe, J.H., Shyshko, S., Roussel, N.. Simulation of fresh concrete flow using discrete element method (DEM): theory and applications. Materials and Structures 2014;47(4):615–630.

[8] Ferraris, C.F., deLarrard F and; Martys, N.S.. Fresh concrete rheology - recent developments. In: Materials Science of Concrete VI. Proceedings. American Ceramic Society. 2001, p. 215–241.

[9] Mori, H., Tanigawa, Y.. Simulation methods for fluidity of fresh concrete. 71-134 44(1); Nagoya University; 1992.

[10] Dufour, F., Pijaudier-Cabot, G.. Numerical modelling of concrete flow: homogeneous approach. International journal for numerical and analytical methods in geomechanics 2005;29:395–416.

[11] Moresi, L., Dufour, F., Mühlhaus, H.B.. A Lagrangian integration point finite element method for large deformation modeling of viscoelastic geomaterials. J Comput Phys 2003;184(2):476–497.

[12] Laure, P., Silva, L., Coupez, T., Toussaint, F.. Numerical modelling of concrete flow with rigid fibers. In: 10th ESAFORM conference on material forming; vol. 907. American Institute of Physics; 2007, p. 1390–1395.

[13] Švec, O., Skoček, J., Stang, H., Geiker, M.R., Roussel, N.. Free surface flow of a suspension of rigid particles in a non-Newtonian fluid: A lattice Boltzmann approach. Journal of Non-newtonian Fluid Mechanics 2012;179:32–42.

[14] Roussel, N.. Rheology of fresh concrete: from measurements to predictions of casting processes. Materials and Structures 2007;40:1001–1012.

[15] Ozyurt, N., Woo, L.Y., Mason, T.O., Shah, S.P.. Monitoring fiber dispersion in fiber-reinforced cementitious materials: Comparison of ac-impedance spectroscopy and image analysis. ACI Materials Journal 2006;103(5):340–347.

[16] Lataste, J., Behloul, M., Breysse, D.. Characterisation of fibres distribution in a steel fibre reinforced concrete with electrical resistivity measurements. NDT; E International 2008;41(8):638 – 647.

[17] Van Damme, S., Franchois, A., De Zutter, D., Taerwe, L.. Nondestructive determination of the steel fiber content in concrete slabs with an open-ended coaxial probe. Geoscience and Remote Sensing, IEEE Transactions on 2004;42(11):2511 – 2521.

[18] Faifer, M., Ottoboni, R., Toscani, S., Ferrara, L.. Nondestructive testing of steel-fiber-reinforced concrete using a magnetic approach. In-

strumentation and Measurement, IEEE Transactions on 2011;60(5):1709 –1717.

[19] Roqueta, G., Jofre, L., Romeu, J., Blanch, S.. Broadband propagative microwave imaging of steel fiber reinforced concrete wall structures. Instrumentation and Measurement, IEEE Transactions on 2010;59(12):3102 –3110.

[20] EHE-08, . Instrucción de Hormigón Estructural EHE-08. 2008.

[21] Popinet, S.. Gerris: A tree-based adaptive solver for the incompressible euler equations in complex geometries. J Comp Phys 2003;190:572–600.

[22] Hu, C.. Rheologie des betons fluides. Ph.D. thesis; L'Ecole nationale des ponts et chaussees; 1995.

[23] Zerbino, R., Barragán, B., García, T., Agulló, L., Gettu, R.. Workability tests and rheological parameters in self-compacting concrete. Materials and Structures 2009;42:947–960.

[24] Feys, D., Verhoeven, R., Schutter, G.D.. Evaluation of time independent rheological models applicable to fresh self-compacting concrete. Applied Rheology 2007;17(5):56244–1/56244–10.

[25] Torrents, J., Blanco, A., Pujadas, P., Aguado, A., Juan-García, P., Sánchez-Moragues, M.. Inductive method for assessing the amount and orientation of steel fibers in concrete. Materials and Structures 2012;:1–16.

[26] Abrishambaf, A., Barros, J.A., Cunha, V.M.. Relation between fibre distribution and post-cracking behaviour in steel fibre reinforced self-compacting concrete panels. Cement and Concrete Research 2013;51(0):57 – 66.

[27] Cunha, V., Barros, J., Sena-Cruz, J.. An integrated approach for modelling the tensile behaviour of steel fibre reinforced self-compacting concrete. Cement and Concrete Research 2011;41(1):64 – 76.

[28] Robins, P., Austin, S., Jones, P.. Pull-out behaviour of hooked steel fibres. Materials and Structures 2002;35:434–442.

[29] Bartos, P., Duris, M.. Inclined tensile strength of steel fibres in a cement-based composite. Composites 1994;25(10):945 – 952.

[30] Parmentier, B., De Grove, E., Vandewalle, L., Van Rickstal, F.. Dispersion of the mechanical properties of FRC investigated by different bending tests. In: Proceedings of the fib Symposium "Tailor Made Concrete Structures". fib Symposium "Tailor Made Concrete Structures"; Taylor & Francis Group; 2008, p. 507–512.

[31] Lee, M., Barr, B.. A four-exponential model to describe the behaviour of fibre reinforced concrete. Materials and Structures 2004;37:464–471.

[32] Ferrara, L., Bamonte, P., Caverzan, A., Musa, A., Sanal, I.. A comprehensive methodology to test the performance of Steel Fibre Reinforced Self-Compacting Concrete (SFR-SCC) . Construction and Building Materials 2012;37(0):406 – 424.

[33] Orbe, A., Rojí, E., Losada, R., Cuadrado, J.. Calibration patterns for predicting residual strengths of steel fibre reinforced concrete (SFRC). Composites Part B: Engineering 2014;58(0):408 – 417.